POLITECNICO DI TORINO
Repository ISTITUZIONALE

Use of Computational Fluid Dynamics for improving freeze-dryers design and process understanding.
Part 2: Condenser duct and valve modelling

(Article begins on next page)

17 May 2024

Special Issue of the 8th International Conference on Lyophilization – Freeze Drying (ISL-FD 2017)

R. Pisano & T. De Beer, Eds
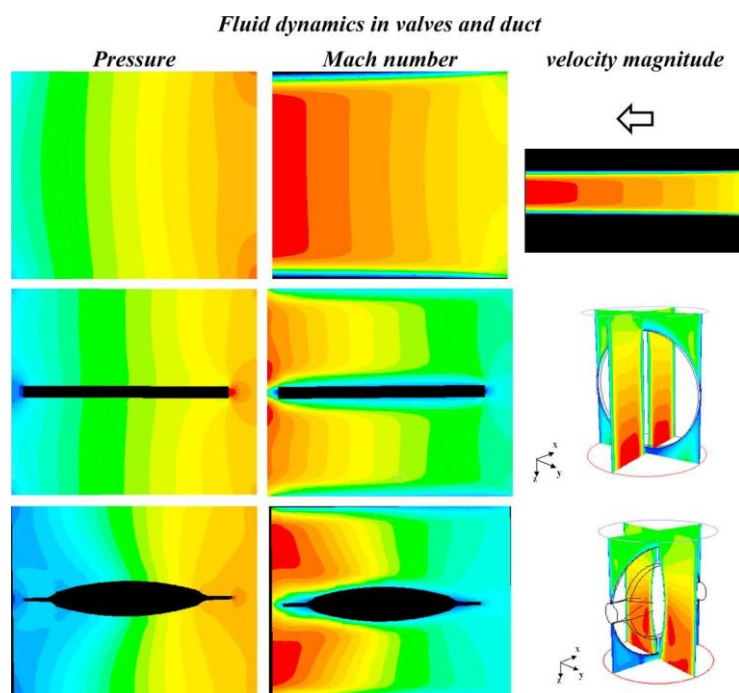
Use of Computational Fluid Dynamics for improving freeze-dryers design and process understanding.
Part 2: Condenser duct and valve modelling

Daniele L. MARCHISIO[1], Miquel GALAN[2], Antonello A. BARRESI[1*]

[1] Politecnico di Torino

Institute of Chemical Engineering - Department of Applied Science and Technology

C.so Duca degli Abruzzi 24, I-10129 Torino, ITALY

[2] Azbil Telstar Technologies, S.L.

Av. Font i Sagué, 55, E-08227 Terrassa, Spain

*Corresponding author: Antonello Barresi (antonello.barresi@polito.it)

authors' e-mail: antonello.barresi@polito.it, mgalan@telstar.com, daniele.marchisio@polito.it

Abstract: This manuscript shows how computational models, mainly based on Computational Fluid Dynamics (CFD), can be used to simulate different parts of an industrial freeze-drying equipment and to properly design them; in particular in this part the duct connecting the chamber with the condenser, with its valves, is considered, while the chamber design and its effect on drying kinetics have been investigated in Part 1.

Such an approach allows a much deeper process understanding and assessment of the critical aspects of lyophilisation. This methodology will be demonstrated on freeze-drying equipment of different sizes, investigating influence of valve type (butterfly and mushroom) and shape on duct conductance and critical flow conditions.

The role of the inlet and boundary conditions considered has been assessed, also by modelling the whole apparatus including chamber and condenser, and the influence of the duct diameter has been discussed; the results show a little dependence of the relationship between critical mass flux and chamber pressure on the duct size.

Results concerning the fluid dynamics of a simple disk valve, a profiled butterfly valve and a mushroom valve installed in a medium size horizontal condenser are presented. Also in these cases the maximum allowable flow when sonic flow conditions are reached can be described by a correlation similar to that found valid for empty ducts; for the mushroom valve the parameters are dependent on the valve opening length. The possibility to use the equivalent length concept, and to extend the validity of the results obtained for empty ducts will be also discussed.

Finally the presence of the inert gas modifies the conductance of the duct, reducing the maximum flow rate of water that can be removed through it before the flow is choked; this also requires a proper over-sizing of the duct (or duct-butterfly valve system).

List of abbreviations
CFD   Computational Fluid Dynamics
CIP   Cleaning in place
DSMC   Direct Simulation Monte Carlo
SIP   Sterilisation in place
TDLAS   Tunable Diode Laser Spectroscopy
QbD   Quality-by-Design

1. Introduction

In freeze-drying the final product quality may be related to the design of the equipment; in fact, the operating conditions are influenced by the design of chamber, duct, valve and condenser, which thus has a strong impact on the flexibility and reliability of the process and on its optimal operation and duration.

For example, the minimum pressure obtainable in the drying chamber and the effectiveness of pressure control depend on the proper sizing of the condenser and of the duct connecting it to the chamber. When transferring the process from one equipment to a different one, and especially when scaling-up from a laboratory or pilot equipment to the industrial one, not only is it necessary to adapt the cycle, but also the equipment must be properly designed to allow maximum sublimation rate and maintenance of the set-point conditions. Process and equipment operation deep understanding is a fundamental requisite to this purpose and a model-based approach was proven to be very useful both for cycle design and process transfer and for equipment design (Fissore et al., 2012a; 2012b; 2015; Barresi and Pisano, 2013).

Not only does the pressure drop across the duct (also called the "throat") influence the minimum chamber pressure, but it might also be used to monitor the process, estimating the sublimation rate; by this way the duct will be transformed in a non-invasive mass flow meter (using the pressure measurements supplied by the pressure gauge usually available in chamber and condenser) and would become a PAT tool useful to pursue a QbD (Quality by Design) approach. The feasibility of this technology has been demonstrated by Patel et al. (2010), who highlighted that a very accurate calibration must be performed at each chamber pressure of interest, as the pressure differences are generally quite small, especially at low Mach number.

The knowledge of the duct conductance is also necessary to build lumped models of the whole apparatus, including chamber and condenser, suitable to investigate the dynamic behaviour of the equipment and the effect of process or freeze-dryer design modifications. Such an approach had been early proposed by Sane and Hsu (2007, 2008). Recently Ganguly et al. (2013) presented a unified simulation framework combining system-level coupled sublimation-condensation model and detailed Computational Fluid Dynamics (CFD) simulations to predict dynamic process conditions as a function of process design. In particular, the effect of load, shelf temperature and chamber pressure on occurrence of choking was discussed using the model of a production-scale freeze-dryer.

The duct conductance, characteristic of each apparatus design, is also the fundamental parameter that, with a lumped dynamic chamber model, allows monitoring of primary drying ("valveless monitoring"), measuring without introducing any disturbance into the process sublimation rate and eventually product temperature (Fissore et al., 2014; Pisano et al., 2016), and accurate estimation of the end of primary drying (Pisano et al., 2009).

The dependence of the duct conductance on pressure, geometry and size of the apparatus, as a consequence of the developing flow conditions, makes the experimental investigation extremely cumbersome and expensive. Resorting to modelling and computation to calculate the correction for developing flow and flow compressibility is thus very advantageous, and the various available approaches have been already reviewed in the Part 1 Introduction.

Direct simulation Monte Carlo (DSMC), which is employable also in the transitional regime,

has been proposed to model the chamber-to-condenser duct both with choked and not choked flows (Alexeenko et al., 2009). Anyway, in the duct the Knudsen number, Kn, is in general sufficiently small to allow the use of CFD, as the flow is commonly in the continuum (laminar) regime, or at most in the early transitional regime for smallest sizes typical of lab scale equipment.

Patel et al. (2010) used a commercial code to estimate the conductance of a duct, with a simplified geometry and simple inlet and outlet boundary conditions (pressures at inlet and outlet were set), comparing simulations with experimental results, obtaining good qualitative results. The work by Patel et al. (2010) evidenced thus that a correlation developed on one freeze-dryer cannot be easily generalized and applied to other freeze-dryers; in addition the real geometry is more complex than that of an empty duct, and the presence of valves, or of tubing for cleaning and sterilisation in place (CIP/SIP) must be taken into account.

CFD has been used extensively to calibrate the Tunable Diode Laser Absorption Spectroscopy system placed in the duct, to measure the sublimation rate (Alexeenko et al., 2009; Ganguly et al., 2012); this tool measures the velocity and the density of the gas in the duct, and from that calculates the mass flux (Gieseler et al., 2007). As the velocity profile is not yet developed, a complex calibration work based on preliminary simulations must be carried out, taking into account also the presence of the CIP/SIP tube which interferes with the velocity profile development and causes flow asymmetry.

CFD has been also employed to model the whole apparatus, to evaluate performance and estimate the minimum reachable chamber pressure; an example of a pilot scale freeze-dryer can be seen in Barresi et al. (2010). Ganguly et al. (2013) used it to evaluate the effect of equipment modifications and valves and baffles positioning, in order to improve process and equipment performance.

Also the design of the condenser can largely benefit from the knowledge of the real fluid dynamics inside the condenser itself and from the evaluation of the ice deposition rate on coils and surfaces: computations can become extremely heavy in this case, especially for the complex geometries of industrial apparatus, due to the necessity of modelling the vapour disappearance (and the ice formation) with a realistic mechanism that takes into account the proper kinetics. CFD can still be employed in many cases and for example has been used to estimate the flow field in condensers of different type and around a mushroom valve (Petitti et al., 2013) or the effect a baffle (Ganguly et al., 2013) at the entrance of a condenser. At lower pressure conditions other approaches more suitable for the transitional and free-molecular regimes, like the DSMC as proposed by Ganguly and Alexeenko (2012), may be preferable; this method resulted also very effective in describing the icing phenomena that occur on the coils of the condenser.

Critical is also the capability of the freeze-dryer to evacuate the requested water vapour flow rate, in order to operate under the desired operating conditions. Typical design parameters that affect the overall performance of the freeze-dryer with respect to these issues are mainly the geometry of the condenser and, for freeze-dryers with condensers separated from the freeze-drying chamber (which is the most common case in industrial apparatuses), the size of the duct and of the isolating valve.

Searles (2004) evidenced the possibility of choked flow and the limitations caused by this phenomenon to the freeze-drying process, reporting experienced failures to maintain product chamber pressure at set-point early in primary drying. Because the condenser pressure remained

significantly lower than the product chamber pressure, the product chamber overpressure events were due to resistance to water vapour flow from the chamber to the condenser. Patel et al. (2010) experimentally investigated the occurrence of choked flow in a small pilot-scale apparatus, showing maps of average sublimation rates *vs.* pressure condenser at different chamber pressures.

Thermodynamic theory shows that for ducts of constant cross-section the maximum possible velocity that can be achieved is Mach 1, that is the speed of sound or sonic velocity (see for example the book by White (2009)). In fact, if the flow velocity is greater than or equal to the speed of sound (e.g. sonic or supersonic flow), then any downstream pressure changes cannot travel upstream or affect the mass flow rate because the pressure disturbance (or pressure wave) travels at the speed of sound. Of course in cases of obstructions, as for examples for the presence of a valve, the fluid dynamics is more complex, and the maximum flow rate is determined by the smallest open section. Notwithstanding the relevance of the phenomenon is nowadays fully acknowledged, and the inclusion of the choked flow curve in the design space is now a common practice (Nail and Searles, 2008; Patel et al., 2010; Fissore et al., 2011), relatively few data and design procedures have been published up to now.

Oetjen (1999, 2004; Oetjen and Haseley, 2004) presented graphic correlations for jet flow and for critical flow in straight ducts, as a function of the length-to-diameter (*L/D*) ratio. The mass flux (which was named in those works "density of water flow") was plotted as a function of the chamber pressure; the values were calculated with the Günter-Jaeckel-Oetjen equation (references are to equation (1.3.11) or its graphical plots (Fig. 1.3.4 or 1.3.6) in Oetjen's book (Oetjen, 1997). By assuming that the mass flux (that is the mass flow rate for unit section) is not affected by size, it is possible to generalise the results obtained, in order to be able to calculate the flow for any section.

The maximum mass flow, rate $\dot{m}_{max}$, in the case of "jet flow" can be calculated using the following equation, where k is the specific heat ratio ($k = c_p / c_v$), while ρ^* and u^* are the density and velocity of the fluid and A^* the restricted section when the flow is sonic (White, 2009):

$$\dot{m}_{max} = \rho^* A^* u^* = P_0 \left(\frac{2}{k+1} \right)^{1/(k-1)} A^* \left(\frac{2k}{k+1} \frac{M}{RT_0} \right)^{1/2} \tag{1}$$

T_0 and P_0 appearing in the formula are the stagnation temperature and pressure, that correspond to inlet temperature and pressure only in the case the initial gas velocity is null (or at least very low, compared to the sonic one). This is generally the case for an orifice in a large vessel, but this case is very different from what happens generally in a duct whose size is comparable with that of the chamber: if the duct is straight, and not very long, then the velocity at the inlet is of the same order of magnitude of that at the exit, even if it increases due the pressure reduction. This is a simplified case, in which only the behaviour along the centreline is considered, not taking into account the effect of the wall, and assuming isentropic behaviour. This is also called "jet flow" because corresponds well to flow condition through a small orifice in a wall.

It is clear that the jet flow calculation is a very approximated evaluation of the maximum allowable flow in a short duct, because the friction effect will reduce it, but the inlet gas velocity also has a strong effect, as shown in Equation (1); unfortunately its consideration makes the solution of the above equation implicit. Anyway, the jet flow regime can be easily calculated by using for example a simple spreadsheet calculator and considering the initial null velocity case, it can be a

rough estimation that can give quickly an upper bounded value, at least for short ducts, as shown in Barresi and Marchisio (2018) [see Figure 2 and 21].

Some simulation results for a tube with a variable number of bends have been reported by Searles (2004), who also proposed, on the base of geometrical considerations, to approximate the behaviour of the valve with that of two bends. The flow in a curved duct may be complicated by the presence of recirculation flow, and is certainly different from that occurring in a valve section; anyway, preliminary results have shown that CFD can be successfully used to predict conductance and critic flow in empty ducts and around valves, but the effect of the valve is more complex than a simple increase in the duct equivalent length (Barresi et al., 2010; Fissore et al., 2015). It must be highlighted that while under moderate operating conditions the flow is generally subsonic and can be described with incompressible CFD solvers, when the operating pressure is significantly reduced and large sublimation fluxes are evacuated from the freeze-drying chamber the Mach number can increase up to unity. These flow conditions can be realistically represented (especially the fate of the fluid while undergoing section changes) with compressible CFD solvers, capable of dealing with sonic and super-sonic conditions.

In Part 1 (Barresi et al., this issue) modelling of the drying chamber has been investigated in detail, addressing the problems of evaluating and reducing batch heterogeneity. The influence of chamber geometry, clearance between shelves and number of shelves, position of the duct leading to the condenser, number and position of the inert gas injection nozzles, as well as temperature gradients of the heating fluid circulating through the shelves have been discussed.

In this paper, conductance of ducts and valves will be studied, evidencing the effect of boundary conditions selected (including the slip or no-slip assumption) and of actual entrance conditions, modelling not only the duct section, but also the actual apparatus. In fact, as already shown in Part 1, entrance effects may be responsible for the largest part of the pressure drop. Relationships for allowed sublimation rate *vs.* chamber and condenser pressure will be presented for empty ducts and butterfly valves of different shape, discussing the validity of the equivalent length concept. A correction factor for the effect of inert gas in the gas mixture will be also presented. Finally, information on the mushroom behaviour will be presented.

2. Governing equations and characteristic flow features

As discussed in detail in Part 1, the fluid dynamics of the vapour in the drying chamber is described by the well-known continuity and momentum balance equations that, written in their general form (by using the Einstein notation) read as follows:

$$\frac{\partial \rho}{\partial t} + \frac{\partial}{\partial x_i}\left(\rho u_i\right) = 0 \tag{2}$$

$$\frac{\partial}{\partial t}\left(\rho u_i\right) + \frac{\partial}{\partial x_j}\left(\rho u_i u_j\right) = -\frac{\partial P}{\partial x_i} + \frac{\partial}{\partial x_j}\left(\tau_{ij}\right) + \rho g_i \tag{3}$$

where ρ is the fluid density, related to temperature and pressure values through the ideal gas law, that is a valid equation of state for the operating conditions investigated in this work, u_i is the ith

component of the fluid velocity, P is the fluid pressure, g_i represents field forces, such as gravity (negligible in this case), and τ_{ij} is the viscous stress tensor, that for Newtonian fluids is usually expressed as a function of the fluid viscosity μ and of the velocity gradient tensor.

Density is evaluated according to the ideal gas law, whereas the viscosity is calculated with the standard kinetic theory (Chapman and Cowling, 1939):

$$\mu = \frac{2}{3} \frac{\sqrt{Mk_B T}}{\sqrt{\pi} d^2} \tag{4}$$

where M is the mass of the molecule (expressed in kg), k_B is the Boltzmann constant ($1.38066 \cdot 10^{-23}$ JK^{-1}), T is the temperature (K) and d is the hard-sphere parameter for the molecule of mass M.

The Knudsen number (Kn) allows to evaluate the fluid dynamics regime; it can be calculated as the ratio of the molecular free path, λ, to a certain representative macroscopic length-scale of the flow, r, that is the diameter (or as suggested by some authors, the radius) in case of a duct or valve (Knudsen, 1909):

$$Kn = \frac{\lambda}{r} \tag{5}$$

When Kn is very small ($Kn < 0.01$) the gas flow is in the continuum regime and the standard continuity and momentum balance equations can be used; but their use can be extended to the so-called transitional regime (for Knudsen numbers bounded between 0.01 and 0.1) solving the continuum CFD equations with partial-slip boundary conditions at the walls (Maxwell, 1879).

Another important dimensionless number is the Mach number (Ma), defined as the ratio between the gas velocity and the sound speed estimated as follows:

$$Ma = \frac{U}{a} = \frac{U}{\sqrt{kRT}} \tag{6}$$

where U is the flow velocity and a is the speed of sound of the fluid ($a = \sqrt{kRT}$). From the ideal gas theory a value $k = c_p/c_v = 4/3$ is assumed for the specific heat ratio of water vapour, as in previous works. It must be noted that the value of the heat capacity ratio for water vapour, 1.33, is lower than that for dry air and nitrogen, that is 1.4; in case of mixtures of nitrogen with water vapour, an intermediate value must be considered.

Under small-Mach number conditions temperature effects can be ignored and density can be assumed nearly constant, whereas for Mach numbers greater than 0.3 there are non-negligible density changes and the equation of state and the energy balance equation are very important. For internal (duct) flows, the most important question to answer is simply whether the flow is subsonic ($Ma < 1$) or supersonic ($Ma > 1$). In fact, for subsonic flows an increase in the section causes an increase in pressure and decrease in velocity, whereas in supersonic flows it causes a decrease in pressure and increase in velocity.

This implies that the fluid can accelerate smoothly through sonic and supersonic flow conditions only in a converging-diverging nozzle (i.e. throat. Another important implication is that the maximum possible mass flow passes through a duct when its throat is at the critical or sonic condition: the duct is then said to be *choked*.

3. Case studies and simulation details

For the duct simulations (either empty or with the butterfly valve), the inlet of the pipe is modelled as a pressure inlet (the stagnation pressure and temperature are imposed and calculated by assuming an isentropic compression), whereas the outlet section is modelled as a pressure outlet (the outlet pressure is imposed), considering for all the cases an inlet static temperature of 239 K.

The simulations are run in the laminar regime with the commercial CFD code Ansys Fluent. A series of simulations three-dimensional in space and steady-state in time have been carried out, considering a constant inlet pressure and different values for the outlet pressure, to examine the effect of reducing outlet pressure on the mass flow in the duct, and then varying the inlet pressure.

3.1. Choked flow in ducts

Different length to diameter ratios (L/D) will be considered: 1.2, 2, 4, 5, 6, 7 and 10, that cover all the range of practical interest; larger L/D values (from 20 to 50) have been also investigated in consideration of the pressure drop values observed in case a valve is present in the duct, to compare them and eventually calculate an equivalent length for the valve. Two duct sizes (DN = 350 mm and 700 mm) have been considered, even if the largest number of simulations has been carried out for the larger duct. The effect of a fraction of inert gas in the vapour flow has been also investigated.

It must be evidenced that certain static pressures, and Mach numbers, have been supposed on the inlet and the relative stagnation conditions have been calculated, but inlet and outlet pressure given at the beginning are considered approximated values, and are adjusted by the code: a relevant number of simulations have been lunched to get a good estimation of the critical conditions.

Due to the low pressure and short residence time, the assumption of adiabatic flow is realistic. Low pressure slip boundary conditions, that should be applied in case of transitional regime (as already discussed in Part 1) have been also tested, but the results confirm that the assumption of viscous flow (and thus the no-slip boundary conditions) are acceptable at least for larger ducts.

A regular (almost flat) velocity profile is considered at the inlet of the duct, as a uniform pressure is imposed. The actual situation may be more complex, but is strongly dependent on the geometry considered, as discussed in Barresi and Marchisio (2018); in any case an almost flat profile at the entrance may be a reasonable approximation for the different cases.
In this work the surface average value will be adopted, but in some examples the radial pressure profile will be also discussed.

3.2. Conductance of butterfly valves

For these simulations, just a short piece of straight duct including the valve has been considered. In detail it is a duct 830 mm long and with a diameter of 700 mm, with a butterfly valve (in open position).

Two different valve shapes have been considered: in a first series of simulations a simplified geometry has been considered, represented by a round disk (685 mm in diameter) with uniform thickness assumed equal to 40 mm, as shown in Figure 1 a).

Then the butterfly valve (again represented in open position) has been reproduced more faithfully to its real geometry (see Figure 1b). The overall diameter of the valve is still 685 mm, but

the valve is represented as the union of three rings of different diameter; geometric details in Barresi and Marchisio (2018).

Also in this case different boundary conditions have been tested; finally correlations have been developed for adiabatic wall and no-slip conditions.

3.3. Simulation of complete equipment

In order to evaluate the influence of actual inlet and outlet conditions on fluid dynamics and flow conductance, some simulations have been carried out on the whole apparatus, including the real chamber and (for the pilot scale) also the condenser. The two freeze-dryer geometries analysed in Part 1 have been considered.

The large scale industrial one has a DN 800 horizontal duct ($L/D = 2$) (see Figure 1 in Part 1); the mass flow rate has been set imposing the sublimation rate on the shelves (the configurations with 14, 15 and 17 shelves have been considered) and the pressure at the duct outlet has been set at 10 Pa.

For the *LyoBeta*^{TM} small pilot-scale equipment (see Figure 7a), two different duct entrances have been compared, a sharp entrance and a rounded one, corresponding to the actual realisation; details of the meshed geometry can be found in Barresi and Marchisio (2018) (Figure 24). A simple flat disk butterfly valve has been considered (see Figure 1 c) for a detail of the duct, ending with a bend in the cylindrical condenser).

The water vapour deposition in the condenser is modelled as a finite rate process taking place on the condenser refrigerated walls (its lateral walls); further details can be found in Petitti et al. (2013). The two chemical species (water vapour and nitrogen) enter the chamber through uniform sources placed on the upper side of four slabs representing the layers of vials, where the inert gas represents the 5% of the overall entering mass flow. In the base case the sublimation rate considered is 1 kg h^{-1}m^{-2}, with an interface product temperature of 239 K., and the pressure of 4 Pa is imposed at the condenser exit (at the entrance of the incondensable gas pipe), modelled as a pressure-outlet.

The low-pressure-boundary slip option is activated in Fluent laminar model, in this case due to the low pressure values and the small duct size.

3.4. Mushroom valve fluid dynamics

A standard horizontal condenser, characterized by a standard toro-spherical bottom (DIN 28011) and a conical inlet, equipped with a mushroom valve, has been considered. The general assemblage is illustrated in Figures 1 d).

The smallest section is at the intersection of the entrance cone with the vessel bottom, and has a diameter $D = 700$ mm; this geometry is compatible with the industrial freeze dryer investigated in Part 1; thus the performances will be referred to the maximum flow estimated for this equipment: in particular the configuration with the maximum number of shelves (17), corresponding to 54 m^2, and the conventional maximum sublimation rate (1 kg/h m^2), leading to 0.015 kg/s will be considered as reference.

The mushroom valve is modelled as a flat disk (diameter = 750 mm; thickness = 80 mm).

The purpose of the CFD simulations is:

- the pressure drop caused by the mushroom valve with different mass fluxes, at a fixed valve distance; to this purpose various mass flow from 0.1 times to the maximum flow rate given above will be considered.
- the pressure drop caused by the mushroom valve in different positions; to this purposes three different distances, l_{valve}, from the vessel bottom will be considered: 215, 250 and 300 mm.

In order to generalise the cases considered, it is important to point out that the minimum reasonable valve distance is the one that does not further reduce the section available for the vapour flow: considering a cylinder having the same diameter of the restricted section and height equal to l_{valve}, it turns out that $l_{\text{valve min}} = D/4$; thus it is convenient to use this value to make dimensionless the valve distance.

Here the same value of stagnation temperature is considered for the different cases, and as a consequence the static temperature may change at the inlet (the variation is of about 5 K between the lowest and the highest flow rate considered). The choice of constant stagnation temperature will allow to have the same static temperature in correspondence of the centre of the disk, where the flow is stopped.

As here the interest is in the detailed investigation of the inlet section, to calculate the resistance and pressure drop caused by the mushroom valve, only the first part of the apparatus will be considered, where there is no ice formation, and thus no material sink. The outlet section, a plane positioned in the vessel behind the mushroom disk, is modelled as a pressure outlet; the outlet pressure is set equal to 4 Pa in all cases and it can be reminded that practically the total pressure is constant in a condenser, as the reduction in partial pressure of water vapour is compensated by the increase in the partial pressure of inert gas (see Figure 24 in Barresi and Marchisio (2018)).

The walls of duct and vessel are modelled as adiabatic surfaces and radiation is neglected.

4. Results and discussion

Choked flow conditions may establish in the duct connecting chamber and condenser. In fact, due to the very low pressure values (and therefore very high water vapour velocities) critical sonic flow conditions may be encountered. The diameter and length of the duct, as well as the geometry of the isolating valve, must be properly designed, in order to guarantee under a wide range of operating conditions that the desired sublimation rate is evacuated.

4.1. Choked flow in straight ducts. Influence of duct diameter. Generalisation of the results.

Two duct diameters have been considered: DN 350 and DN 700, corresponding to those largely used in medium size and large apparatus.

Figure 2 (upper graph) shows the dependence of the vapour mass flow rate on the outlet (condenser) pressure, with the inlet (chamber) pressure as a parameter, for the larger size. The surface average pressure is considered.

The zone where the mass flow becomes independent of the outlet pressure is clearly visible, and is extended by the dashed line. The open symbols refer to pressures slightly higher than the others of the series, for which the expected flow rate is higher (the inlet pressure cannot be set exactly in the simulations).

The critical flow depends on the chamber pressure, similarly to what previously observed for the simplified case of "jet flow". The data can be also plotted versus the chamber pressure, with the condenser pressure as a parameter: this is shown in Figure 2 (middle graph). Here the line of the sonic flow condition is continuously increasing and represents the asymptote of the curves obtained for different outlet conditions. A similar plot for the smaller duct size can be seen elsewhere (Fissore et al., 2015).

Comparing the mass flux calculated for the two diameters, at a first glance it appears that the results are practically equivalent. The bottom left graph in Figure 2 compares the critical mass flux for the two diameters, evidencing that the duct diameter actually has an influence, even if quite small, as the friction at the wall plays a minor role in this case. It can be seen that for the critical flow case, the correction for the smaller duct is less than 7%: in terms of equivalent length, it appears that the duct with DN 350 behaves like that having DN 700, but with a longer length (*L/D* about 4).

Figure 3a shows an example of design charts for chocked flow conditions. It highlights the influence of the *L/D* ratio on mass flow, at different chamber pressure. An alternative plot is shown in Barresi and Marchisio (2018) (Figure 20).

4.1.1 Effect of the inert gas fraction

It is known that the relationship between pressure drop and flow rate, and the maximum allowed flow in choked conditions, depends on the characteristics of the compressible gas; this can be easily shown for jet flow conditions, and has been confirmed by experimental results carried out in the small pilot freeze-dryer (data not shown).

The case of jet flow can be treated analytically, using Equation (1), and it is useful in order to get some general trends, even id data obtained must be treated with caution, to avoid conceptual errors; anyway, it will be shown that the qualitative conclusions obtained for jet flow can be applied to any duct flow, and thus for design purposes calculations can be carried out using the simpler approach discussed below, and a simple spreadsheet calculator. Some results are shown in Figure 21 of Barresi and Marchisio (2018).

Qualitatively the results obtained for water-inert gas mixtures are very similar to those obtained for pure water, but the total mass flux increases in presence of inert gas: this is expected because it is known that the maximum conductance is higher in case of nitrogen than for water vapour. The critical mass flux increases with the initial Mach number; it can be reminded that, as a first approximation, the case of jet flow at Mach = 0.5 might corresponds to the case of a short duct. The critical mass flux increases progressively when the fraction of nitrogen gas increases. But it must be taken into account that the mass flux of the mixture is strongly affected by the different molecular weigh of nitrogen and water. If the critical molar flux is considered, the conclusions are reversed, as the molar flow rate is higher for pure water vapour and decreases more than proportionally when the inert gas fraction increases. It must be evidenced that even if the total mass flux increases, the water mass flux decreases in presence of inert gas.

If the behaviour of straight ducts is analysed, using CFD simulations, similar results are obtained, as can be seen in Figure 2 (bottom right); this means that in presence of a pressure control by controlled leakage, the duct size must be oversized. What is very interesting is that in terms of relative flow rate of water, the results are in very good agreement with those obtained by the simple

calculation for jet flow. Thus the results obtained by CFD in the different configurations for water vapour, can be easily generalized to water-inert gas mixtures using the relationship shown in Figure 2. If the described use can be advantageous, on the other and the results obtained by simple jet flow calculations can be misleading; in particular the graphical solutions often reported (included those given by Oetjen in his books) generally correspond to the jet flow solution for water vapour at 0°C and zero inlet velocity, that are not fully appropriate for the duct to the condenser.

4.2. Butterfly valve

The conductance of the duct can be significantly modified by the presence of a valve. Even if this is well known, and the problem of choked flow and loss of pressure control in the chamber is very often reminded in the scientific literature, very few data are actually available, as already discussed in the Introduction.

On the other hand the choice of the right size for the duct (and thus for the valve) is considered of great importance in designing the apparatus, and the size of the duct is also one of the most relevant aspects to be considered in process transfer.

In spite of these considerations, the only quantitative data published refer to straight ducts, or at most to ducts with bends. As said before, the approach proposed is to consider an equivalent length for the valve, in order to use the available data obtained for ducts. Unfortunately no data about the equivalent length of valves is available in the open literature and it has not been even proved that the approach is correct.

In Oetjen and Haseley (2004) just a few comments can be found: it is assumed that the pressure drop connected with a mushroom valve is very low, and it is suggested that it can correspond to a duct with $L/D = 1.6$. No clear data are given for the butterfly valve; but from the analysis of a real apparatus, as it will be shown in the followings, it comes out that the valve may correspond to a duct with $L/D \sim 20$.

Two different geometric configurations have been considered here: this will also allow an evaluation of the influence of the geometric details.

4.2.1. Flat disk valve

The simple disk valve shown in Figure 1a) has been considered first; qualitatively the mass flux-pressure relationships are similar to those of the empty ducts.

Data can be generalised using the mass flux, as for the duct, even if a dependence on the diameter is expected. It can be noted that decreasing the outlet pressure, the mass flux reaches a maximum and constant value, corresponding to choked flow (see Figure 3b).

If the inlet pressure is increased, keeping constant the outlet pressure, the mass flow increases, and keep increasing also after that choked conditions are obtained. An example is shown in Barresi and Marchisio (2018) (Figure 4) for different boundary conditions.

The significant reduction of the conductance due to the presence of the disk may be explained in part with the reduction of the section available, and with the obstacle caused by the disk itself, but as the pressure drop in the duct is mainly related to the inertia effect due to the developing of the velocity profile, in the butterfly valve the increase may be explained with the larger modification of the velocity profiles.

4.2.2. Profiled butterfly valve

Qualitatively the results are similar to those obtained with the simple disk valve, even if the conductance in this case is lower (that is the vapour mass flow allowable is lower, for the same chamber pressure); also transition to choked flow condition takes place at lower chamber pressure (see Figure 3b). It must be noted that in this case the minimum open section is smaller in the profiled valve, even if the thickness at the outer border is smaller.

Figure 4 shows an example of the contours of pressure and Mach number and a comparison with the flat disk case, for a flow condition not far from the critical one; velocity and temperature profiles for the same cases, and with various different boundary conditions, can be found in Figure 22 in Barresi and Marchisio (2018). The differences in the pressure and velocity profiles, consequences of the different valve geometry, are evident; it can be also noted that while with the flat disk the maximum velocity was obtained at the exit from the valve zone, in this case, as the open section is not constant, the maximum velocity is observed after the restricted section.

The whole set of results obtained in chocked flow conditions for the two butterfly valves with different disk geometry is shown in Figure 5 (upper graph). As said, the simulations have been carried out for DN 700, but the results have been generalised using the mass flux concept. It is evident that the conductance of the two valves is significantly different: the geometry corresponding to the flat disk allows larger vapour flow rates.

It was anticipated that the use of the equivalent length concept, to take into account the effect of the butterfly valve, may be questionable, and in any case no reliable data were available up to now. The results of the CFD simulations confirm this, showing also that the resistance due to the valve is always very significant, and in practice, for cases corresponding to common commercial freeze-dryers, where the length of the duct is kept at a minimum (generally L/D is in the range 1.2 to 2, and is lower than 3 also in vertical installations) the flow conductance is determined by the valve. Thus, for design purposes, in case a butterfly valve is present, the design charts developed for the valve can be used for the whole line, independently of the real duct length (even if the simulations have been carried for a geometry that includes only a short duct length, with $L/D = 1.186$).

Anyway, if the concept of equivalent length for the butterfly valve were demonstrated to be valid, it could be used to extend the application of the results and charts developed for straight empty ducts. Unfortunately, it appears that the slope of the line that represents the behaviour of the valve is different from the slope of the many lines that represents the tubes, shown in Figure 20 in Barresi and Marchisio (2018). The slope is higher in the case of the valves; this implies that the effect of the valve – that is, the pressure drop it produces – cannot be simply modelled by a certain piece of straight tube, as the equivalent length would increase with the inlet pressure considered.

It can also be noted that the behaviour of the two valves, differing for the shape of the disk, is different: in the range considered, from 6 to 40 Pa, the equivalent length of the valves increases from about 4 to about 12 L/D, and from about 6 to about 40 L/D for the flat disk and profiled disk valve respectively, if the maximum flow in choked flow conditions is considered (see Figure 5, bottom graph).

4.3. Simulation of real freeze-dryers

In the previous section results for empty ducts and butterfly valve have been presented, obtained imposing reasonable but ideal inlet and outlet conditions, that is a flat pressure profile; the mass flow rate has been calculated, as the inlet velocity profile, that is obviously symmetric. Actually, as discussed in Part 1, the real situation may be different, and strongly depends on the geometry of the whole apparatus. Considering the large-scale industrial apparatus investigated in Part 1, the flow field in the chamber is complex [see Figure 9 in Barresi and Marchisio (2018)] and a strong change in the direction of the velocity vectors occurs at the duct inlet; as a consequence a significant pressure drop may take place in the lateral clearance zone close to the duct (see Figure 4 and 6 in Part 1), where vertical pressure gradients are also present. As the overall inlet effects in the duct are responsible for the largest part of the pressure drop, it is evident that the velocity and pressure profiles at the entrance may significantly affect the actual duct conductance.

Thus in this section the two real cases, corresponding to the industrial apparatus and to the lab-scale freeze-dryer will be investigated in detail, modelling the chamber-duct system together (and for the lab-scale including also the condenser to simulate real outlet conditions). Additional results can be also found in Barresi and Marchisio (2018) (section 3.8).

4.3.1 Inlet effects in the large-scale apparatus

As concerns the large-scale apparatus, just a straight duct, with a $L/D = 2$ has been considered, even if in the real cases some conical connections can be used at the end (the real geometry has been considered for the modelling of the mushroom valve). That because we wanted to focus just on the possible inlet effect, avoiding disturbances from the outlet; a reasonable duct length has been considered, sufficient to allow, at least in part, the development of the velocity profile. A sketch of the apparatus, with the exact location of the planes where radial pressure and velocity profiles are given is shown in Barresi and Marchisio (2018) (Figure 22a). Figure 6 (upper graph) shows the radial profile of pressure along the duct; it can be noted that at the inlet the pressure profile is very far from being flat, as supposed in the simple duct simulations carried out by us and other authors, and is also non-symmetric; this is related to the situation in the chamber (the profile in the midplane of the clearance zone is also shown). The profile is evaluated on the vertical plane passing for the centreline of the duct, but the differences in the *x*-direction are more limited (a 3D contour plot is shown in Figure 22b in Barresi and Marchisio (2018)). The pressure profile is still asymmetric (even if almost linear) after 1/3 of the duct and is almost flat, even if irregular at 2/3 of the duct; but it must be reminded that the flat profile at the outlet has been imposed.

4.3.2. Conductance of the lab-scale freeze-dryer. Influence of the shape of the entrance

Two different entrances have been compared for the *LyoBeta* freeze-dryer: a sharp entrance and a rounded one. Figure 6 (bottom graphs) shows the pressure radial profile at different positions along the *z*-axis: in the chamber clearance zone below the bottom shelf (the first four curves) and then in the first section of the duct, from the inlet to the butterfly valve, generally every 10 mm (further geometrical details in Barresi and Marchisio (2018)). A sketch of the whole apparatus is also shown in Figure 7a, while in Figure 7b an example of the fluid dynamics is presented, evidencing the strong acceleration of the flow after the valve restriction and the jet entering the condenser.

In this case the duct is vertical and in the bottom of the chamber, but qualitatively the behaviour of the pressure profiles is very similar to that observed in the previous case: the profile has a double maximum at the entrance, the minimum becomes deeper at the beginning of the duct and the profile becomes almost flat at half length (z/D approximately 0.6-0.7). In the last section a new minimum is formed in this case, for the presence of the valve, that becomes stronger and stronger (close to the edge of the disk the difference between centre and border value is higher than 2 Pa). Thus in this case the contour pressure value decreases along the duct, but the centreline value has a non-monotonic behaviour (see Figure 24e in Barresi and Marchisio (2018)), similarly to the average pressure.

The pressure drop is higher in the case of a sharp entrance and also smaller radial gradients are observed. As concerns the velocity profile (see Figure 24b in Barresi and Marchisio (2018)), the shape of the entrance has also an effect on the radial profiles; higher velocities are observed with the sharp entrance.

Figure 7c shows the mass flux in the duct of the lab-scale freeze dryer, as a function of the chamber and condenser pressure. Anyway, no assumptions on the pressure and velocity profiles at the entrance or exit of the duct have been made in this case; in fact, the pressure is set at the condenser exit, but simulations have confirmed that no significant pressure drop occurs in the condenser cylinder: a linear variation of the partial pressure of water and inert gas is observed (see Figure 24g and section 3.8.3 in Barresi and Marchisio (2018) for additional information on the behaviour of the cylindrical condenser). The sublimation rate is fixed in correspondence of the shelves, and thus the total mass flow rate (a fraction of 5% inert gas is also considered); the reference pressure in the chamber, established as a consequence of the pressure drop across the duct, is evaluated and used for the correlation.

The general trend is similar to that obtained for ducts and butterfly valves with simplified boundary conditions, but in this case the conductance is significantly lower than that estimated for the large valve (compare values in Figure 3); this can be explained considering the small diameter (DN 100), the longer duct with bends, the presence of inert gas (the water mass flux is shown), and the different boundary conditions.

4. 4. Pressure drop with mushroom valves

As said before, few data are available concerning the pressure drop trough a mushroom valve, even if it is generally assumed that it is small. Actually, the resistance to flow due do the mushroom valve can be comparable to that of a butterfly valve, but for sufficiently long valve opening distances lower values can be obtained; the resistance is anyway stronger than reported up to now.

The vapour flow is practically stopped by the valve disk: the gas is diverted and accelerated laterally; the highest velocity is reached around the disk. Figure 8d evidences the zone where the flow is supersonic: critical flow conditions (corresponding to the yellow zones) are reached in the outer zone just at the inlet in the vessel bottom, after the connection with the duct, and then in the annular region around the valve disk; as seen before, in this zone the highest velocities are obtained, and Mach in the case considered reaches the value 1.8.

CFD results, showing the general fluid dynamics in the apparatus, can also suggest design modifications. In this case it can be observed that the vapour passes preferentially in the outer zone of the tube bundle. This gives a good advice about modifying the system in order to favour a better

distribution of the condensing vapour and thus to improve the condenser efficiency. To this purpose for example Ganguly et al. (2013) analysed the effect of a baffle inserted between the valve disk and the condenser.

An example of the pressure distribution in the system, for different values of the sublimation rate, is shown in Figure 8 a) and b). It can be noted that, as expected, the strong reduction in velocity caused by the presence of the disk corresponds to a significant increase in the absolute pressure, that locally can be higher than the inlet value. In all cases it is evident that the pressure drop is localised in correspondence of the disk, and the pressure in the planes behind the disk is quite uniform, and close to the exit value.

Figure 8 also shows the contour plots of the absolute pressure for two different configurations, evidencing that the valve distance significantly affects the pressure drop, and in particular the pressure in the inlet zone: the shorter the valve distance (that is the smaller the clearance for the passage of the vapour) the higher the pressure at the inlet; differences in the rear zone are much weaker.

Further data on velocity profile and pressure distribution for the mushroom valve with different configurations and operating conditions are available in Barresi and Marchisio (2018).

The data obtained from CFD simulations have been analyzed in order to recover information suitable for pressure drop prediction and to develop a design correlation for maximum allowable flow, depending on the valve configuration. For these purposes the average surface pressure in the inlet and outlet sections has been calculated.

Figure 9a shows that the inlet pressure (for a constant condenser pressure, taken equal to 4 Pa) increases linearly with the sublimation rate in the industrial scale freeze-dryer chamber, at least in the upper range considered, and the slope is dependent on the disk valve distance. The same data can be seen in terms of pressure drop as a function of the valve distance. From the data it appears that the pressure drop may be significant, and that high values of sublimation rate (at full loading) may be not compatible with the maintenance of a low chamber pressure. The data evidence that a linear relationship exists between the inlet pressure and the critical mass flux. Thus, the general behaviour is very similar to that described for the empty duct and the butterfly valves (see Figure 31 in Barresi and Marchisio (2018)).

As the mushroom valve is generally considered a device that causes lower pressure drop than the butterfly valve, it is interesting to compare its behaviour with that of the butterfly valve investigated in the previous sections. A comparison can be done also with empty ducts of different length, to evaluate if the mass flow density *vs*. inlet pressure relationship is similar, and thus the equivalent approach can be adopted. In all cases ducts and valves of the same nominal diameter (DN 700) will be compared. Figure 31 in Barresi and Marchisio (2018) shows that the conductance of mushroom and butterfly valves is comparable, and depending on the geometric details, higher or lower mass fluxes can be obtained. It appears in particular that the conductance of the simple butterfly valve with flat disk in intermediate between that of the mushroom valve with smallest and largest clearance, while that of the butterfly valve with profiled disk is smaller.

As concerns the comparison with an empty duct, it appears that the conductance of the mushroom valve is lower than that of a duct with $L/D = 1.6$ as previously suggested by Oetjen (1999) (at least for the clearances considered in this work) but, depending on the disk valve distance, may be comparable with a duct having a length/diameter ratio in the range $3 - 10$.

As a first approximation, the conductance of the mushroom valve with a 215, 250 and 300 mm disk valve distance can be considered equivalent to that of a duct having L/D equal respectively to about 10, 5 and 3.5. The data show also that the actual slope of the duct relationships is slightly different from that of the mushroom valve; thus the correct equivalent length would be dependent on the conditions considered, as already observed for the butterfly valve, even if in this case the variation is smaller.

The CFD simulations allow also the evaluation of the drag force on the disk. To this purpose the net pressure force and the net viscous force on each surface have been considered to calculate the net total force; the viscous contributions resulted generally negligible, anyway. The flow in the entrance of the condenser is quite complex, but resembles the case of the so-called "external flow case" with unrestricted flow moving around a flat disk with the large flat face impacted perpendicularly by the flow. Solutions are given in the literature for a similar geometry, but here the case is more complex because the flow is compressible and restricted by the condenser shell, of variable section. The force on the disk is mainly due to the difference in pressure between the front and the rear faces, and is strongly influenced by the velocity profiles around the disk.

At low velocity and with the lowest clearance, a recirculation zone is clearly evident around the disk (see Petitti et al. (2013)). Increasing the velocity, and reducing the space between the disk and the tube bundle, the recirculation zone practically disappears. The resultant drag force on the disk, F_d, obtained from CFD simulations, is shown in Figure 9b, for different valve disk distances: the force is higher when the clearance is smaller. Introducing the dimensionless drag coefficient, C_D, the force can be calculated from the force data using the following relationship:

$$F_d = \frac{1}{2} C_D A \rho_{in} U_{in}^2 \tag{7}$$

where A is the projected area of the object (in this case the disk) in direction of the flow, while ρ_{in} and U_{in} are respectively the density and the gas velocity at the inlet, obtained from CFD simulations.

Figure 9c shows the dependence of the drag coefficient on the Reynolds number, $Re = U_{in} D/v$, defined in terms of inlet velocity and valve disk diameter, D; the kinematic viscosity, v, has been calculated with the kinetic theory of gases. The drag coefficient increases with Re in the range considered, a behaviour characteristic of disks in an intermediate Reynolds range.

5. Conclusions

The investigation of the internal fluid dynamics in a freeze-dryer solely relying on experimental techniques is difficult, very costly and time consuming; therefore the use of computational models is an interesting alternative.

CFD can be employed to predict the fluid dynamics in the chamber and duct of freeze-dryers in a wide range of operating conditions of practical interest; its use has also been recently experimentally validated by Sane et al. (2017) comparing measured and predicted pressure profiles over a shelf. Coupled with a model for the product drying in a multi-scale approach it can allow evaluation of the influence of fluid dynamics on process evolution and product quality.

In this work the potentials of CFD in the field of lyophilisation of pharmaceutical products has been deeply investigated, showing how the results can be used in a QbD perspective, to get a deeper

process understanding, to improve equipment performance at the design stage and to avoid errors in operation. Table 1 summarises the tools analysed and their possible applications.

Table 1. Possible applications of the different CFD tools.

	equipment design	process monitoring	batch variance reduction or estimation	process understanding & optimization	scale up
CFD chamber (steady state)	x	x	x	x	x
chamber dynamic response		x			x
CFD duct and valves	x	x			x
chamber multi-scale modelling			x	x	x
condenser modelling	x				x

In the first part of the work, it has been shown how the knowledge of the fluid dynamics in the chamber, and the distribution of inert gas (fed for pressure control) and solvent vapour may be useful for the correct positioning of the monitoring sensors, and for the interpretation of their readings. Two-way coupling between fluid dynamics and process rate was investigated by using a multi-scale model, showing how it can be used to estimate the effect of equipment design and operating conditions on the batch variance.

In this paper the choked flow has been investigated; the role of the inlet and boundary conditions considered has been assessed, and the influence of the duct diameter discussed. The results showed a little dependence of the relationship between critical mass flux and chamber pressure on the duct size; but at least for design purposes the results obtained can be used for the sizes of practical interest, eventually including a small safety factor.

Critical flow behaviour in the connecting duct, in presence of mushroom and butterfly valves, has also been investigated, evidencing the relevance of valve shape and of proper equipment design. CFD results have also shown that some simple design criteria proposed to take into account the presence of the valve can largely underestimate the effects, and more accurate results may be very useful to avoid design errors and consequent process failures.

The possibility to use the equivalent length concept, and to extend the validity of the results obtained for empty ducts has been discussed: even if there is not a perfect correspondence with the behaviour of a duct, as a rough approximation this concept can be used for a first estimate.

It must be evidenced that the results presented and the design chart proposed are valid for the valve geometry considered, and in particular for a mushroom valve realised with a simple thick and flat disk; special disk profiles can reduce the disk resistance increasing the valve conductance. In any case it must always be reminded that the conditions imposed when simulating a simple duct or just the valve section are idealised, and the actual conductance can be significantly influenced by the real entrance conditions. Anyway CFD allows also the simulation of the whole apparatus, thus taking into account the real fluid dynamic conditions, and examples have been shown including also the condenser.

Finally, the presence of the inert gas modifies the conductance of the duct, reducing the maximum flow rate of water that can be removed.

Acknowledgements

Supplementary material

Supplementary material and supporting data have been published in a *Data in Brief* paper (Barresi and Marchisio (2018).

References

Alexeenko A.A., Ganguly A., Nail S.L., Computational analysis of fluid dynamics in pharmaceutical freeze-drying. J. Pharm. Sci. 98(9) (2009), 3483–3494. [DOI: 10.1002/jps.21862]

Barresi A.A., Marchisio D.L., Computational Fluid Dynamics data for improving freeze-dryers design, Data Brief (2018), submitted.

Barresi A.A., Pisano R., Freeze drying: Scale-up considerations, in: J. Swarbrick (Ed.), *Encyclopedia of Pharmaceutical Science and Technology*, 4th ed., CRC Press (Taylor and Francis Group), New York, 2013, pp. 1738-1752. [DOI 10.1081/E-EPT4-120050279]

Barresi A.A., Fissore D., Marchisio D.L., Process Analytical Technology in industrial freeze-drying, in: L. Rey and J. C. May (Eds.), *Freeze-Drying/Lyophilization of Pharmaceuticals and Biological Products*, 3rd rev. Edition, Informa Healthcare, New York, 2010, Chap. 20, pp. 463-496.

Barresi A.A., Rasetto V., Marchisio D.L, Use of Computational Fluid Dynamics for improving freeze-dryers design and understanding. Part 1: Modelling the lyophilisation chamber, Europ. J. Pharm. Biopharm., this issue.

Chapman S., Cowling T.G., *The Mathematical Theory of Non-uniform Gases*, Cambridge University Press, Cambridge, U.K., 1939.

Ferziger J.H., Peric M., *Computational Methods for Fluid Dynamics*, Springer. Berlin, Germany, 2002.

Fissore D., Pisano R., Barresi A.A., Advanced approach to build the design space for the primary drying of a pharmaceutical freeze-drying process, J. Pharm. Sci. 100(11) (2011), 4922-4933. [DOI: 10.1002/jps.22668]

Fissore D., Pisano R., Barresi A.A., A model-based framework for the analysis of failure consequences in a freeze-drying process, Ind. Eng. Chem. Res. 51(38) (2012a), 12386-12397. [DOI: ie-2012-00505n]

Fissore D., Pisano R., Barresi A.A., A model based framework to optimize pharmaceuticals freeze-drying, *Drying Technol.* 30 (2012b), 946-958. [DOI: 10.1080/07373937.2012.662711]

Fissore D., Barresi A.A., Pisano R., Method for monitoring primary drying of a freeze drying process, European Patent EP 2148158 B1 (Published 19.03.2014).

Fissore D., Pisano R., Barresi A.A., Using mathematical modeling and prior knowledge for QbD in freeze-drying processes, in: F. Jameel, S. Hershenson, M. A. Khan, S. Martin-Moe (Eds), *Quality by Design for Biopharmaceutical Drug Product Development*, *AAPS Advances in the Pharmaceuticals Sciences Series 18*, Springer Science+Business Media, New York, 2015, Chap. 23, pp. 565-593. [DOI: 10.1007/978-1-4939-2316-8_23]

Ganguly A., Alexeenko A.A., Modeling and measurements of water–vapor flow and icing at low pressures with application to pharmaceutical freeze-drying, Int. J. Heat Mass Transfer 55 (2012) 5503–5513. [DOI: 10.1016/j.ijheatmasstransfer.2012.05.021]

Ganguly A., Nail S.L, Alexeenko A.A., Rarefied gas dynamics aspects of pharmaceutical freeze-drying, Vacuum 86(11) (2012), 1739–1747. [10.1016/j.vacuum.2012.03.025]

Ganguly A., Alexeenko A.A., Schultz S.G., Kim S.G., Freeze-drying simulation framework coupling product attributes and equipment capability: Toward accelerating process by equipment modifications, Europ. J. Pharm. Biopharm. 85(2) (2013), 223-235. [DOI:10.1016/j.ejpb.2013.05.013]

Gieseler H., Kessler W.J., Finson M., Davis S.J., Mulhall P.A., Bons V., Debo D.J., Pikal M.J., Evaluation of tunable diode laser absorption spectroscopy for in-process water vapor mass flux measurements during freeze drying, J. Pharm. Sci. 96(7), (2007), 1776–1793. [DOI: 10.1002/jps.20827]

Knudsen M., Die Gesetze der Molekularströmung und der inneren Reibungsströmung der Gase durch Röhren, Annal. Physik 333 (1909), 75–130.

Maxwell J.C., On stresses in rarefied gases arising from inequalities of temperature. Phil. Trans. Royal Soc. London 170 (1879), 231–256.

Nail S.L., Searles J.A., Elements of quality by design in development and scale-up of freeze-dried parenterals, Biopharm. Int. 21 (2008), 44–52.

Oetjen G.-W., *Gefriertrocken*, VHC, Weinheim, Germany, 1997.

Oetjen G.-W., *Freeze-Drying*, Wiley-VHC, Weinheim, Germany, 1999.

Oetjen G.-W., Industrial freeze-drying for pharmaceutical applications, in: L. Rey and J. C. May (Eds.), *Freeze-drying/lyophilization of pharmaceutical and biological products*, 2nd Edition, Marcel Dekker Inc., New York, 2004, Chap. 15, pp. 425-476.

Oetjen G.-W., Haseley P., Freeze-Drying (2nd edition), Wiley-VHC, Weinheim, Germany, 2004.

Patel S.M., Chaudhuri S., Pikal M.J., Choked flow and importance of Mach I in freeze-drying process design. Chem. Eng. Sci. 65(21) (2010), 5716–5727. [DOI: 10.1016/j.ces.2010.07.024]

Petitti M., Barresi A.A., Marchisio D.L., CFD modelling of condensers for freeze-drying processes. Sādhanā (Bangalore) – Acad. Proc. Eng. Sci. 38(6) (2013), 1219-1239. [DOI:10.1007/s12046-013-0155-z]

Pisano R., Guler S.B., Barresi A.A., In-line detection of Endpoint of sublimation in a freeze-drying process, In: *Proceedings of the European Drying Conference AFSIA 2009*, Lyon, France, 14-15 May 2009. *Cahier de l'AFSIA* Nr 23 (2009), pp. 110-111.

Pisano R., Fissore D., Barresi A.A., Non-invasive monitoring of a freeze-drying process for *tert*-butanol/water cosolvent-based formulations, Ind. Eng. Chem. Res. 55(19) (2016), 5670-5680. [DOI 10.1021/acs.iecr.5b04299]

Sane S.V., Hsu C.C., Strategies for successful lyophilization process scale-up (Short Survey), Am. Pharm. Rev. 19(1) (2007), 132-136.

Sane S.V., Hsu C.C., Mathematical model for a large-scale freeze drying process: A tool for efficient process development & routine production, in B. N. Thorat (Ed.), *Drying 2008 - Proceedings of the 16th International Drying Symposium (IDS2008)*, Hyderabad, India, 9-12 November 2008, Vol. B, pp. 680-688.

Sane P., Varma N., Ganguly A., Pikal M., Alexeenko A., Bogner R.H., Spatial variation of pressure in the lyophilization product chamber part 2: Experimental measurements and implications for scale-up and batch uniformity, AAPS PharmSciTech. 18(2) (2017), 369–380. [DOI: 10.1208/s12249-016-0502-6]

Searles J., Observation and implications of sonic water vapour flow during freeze-drying, Am. Pharm. Rev. 7(2) (2004), 58–69.

White F., *Fluid Mechanics*, 7th Ed., McGraw-Hill, New York (NY), U.S.A., 2009.
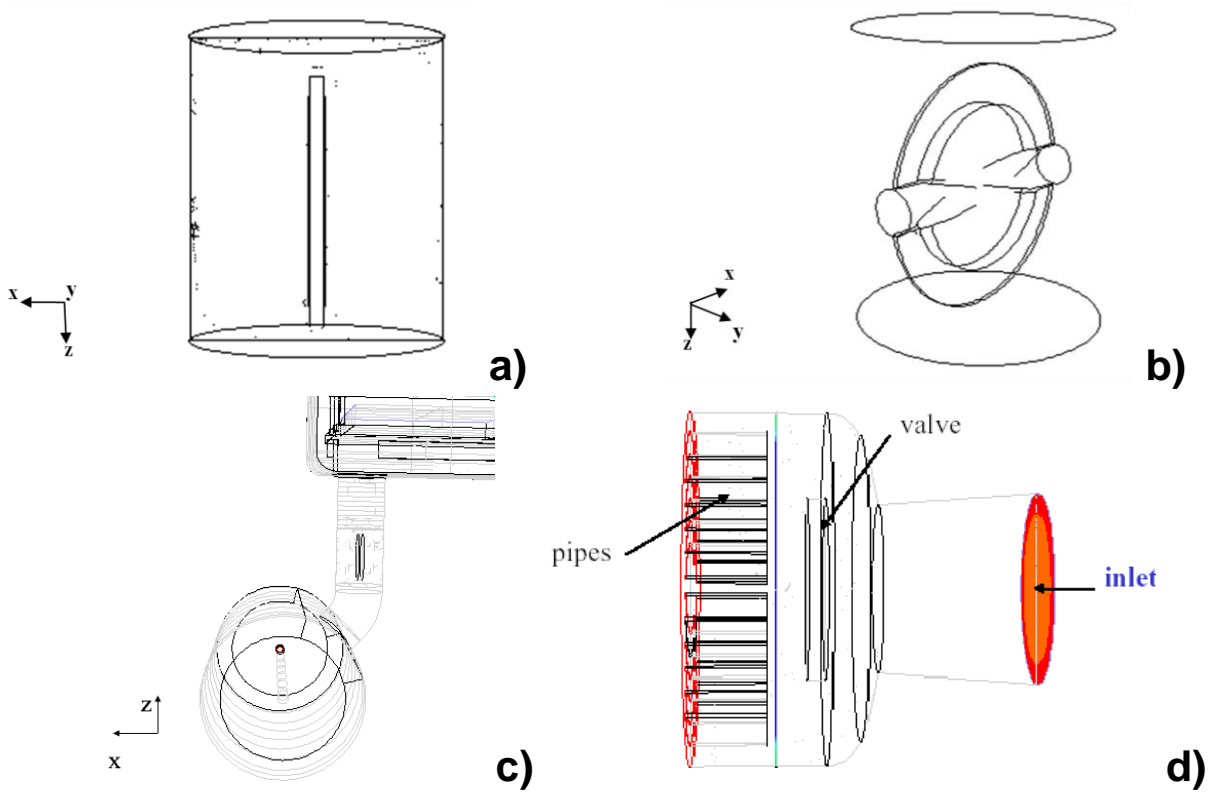
Figure 1. (a) Geometry of the disk valve and (b) of the profiled butterfly valve considered in the simulations; duct inlet on top (at the lowest z value), duct outlet on the bottom.
(c) The actual duct with the butterfly valve, connecting the chamber and the condenser in the lab scale apparatus.
(d) Geometry considered for the CFD simulations of the mushroom valve, including the converging duct and the very first part of the tube bundles.
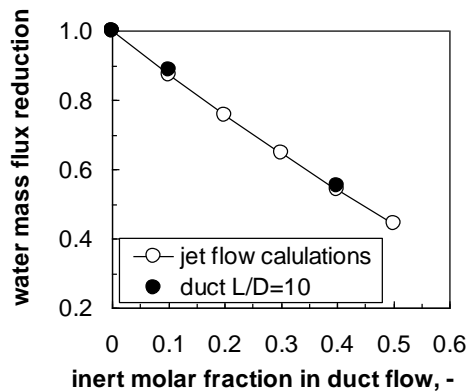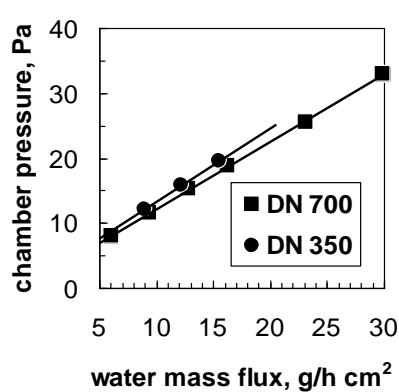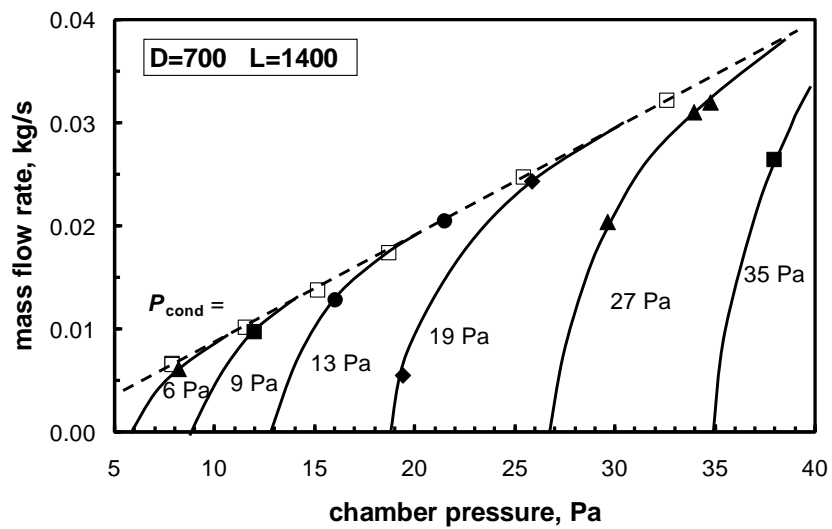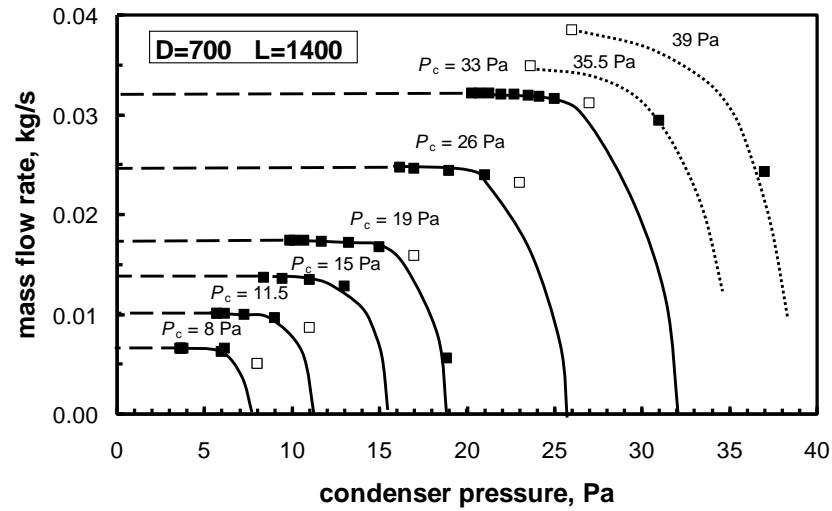
Figure 2. Upper graph: water mass flow rate as a function of the condenser pressure for different chamber pressures, P_c. The transition to sonic flow condition, with constant mass flow rate, is indicated by the dashed line. Middle graph: water mass flow rate as a function of the chamber pressure for different condenser pressures, P_{cond}. The dashed line with open symbols represents the asymptote and corresponds to sonic flow. Straight duct, DN 700, L =1400 mm (L/D =2).

Bottom graph, left: critical water mass flux as a function of the chamber pressure for different duct diameters (L/D=2). Bottom graph, right: reduction in the critical water mass flux as a function of the inert gas fraction in mixture for jet flow and a long duct (the actual value divided by the value with no inert gas is plotted). From simulations with no-slip and adiabatic wall boundary conditions.
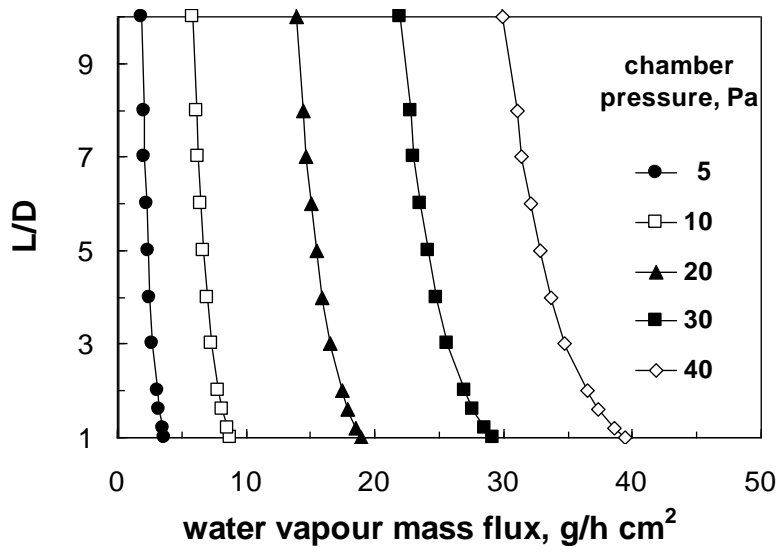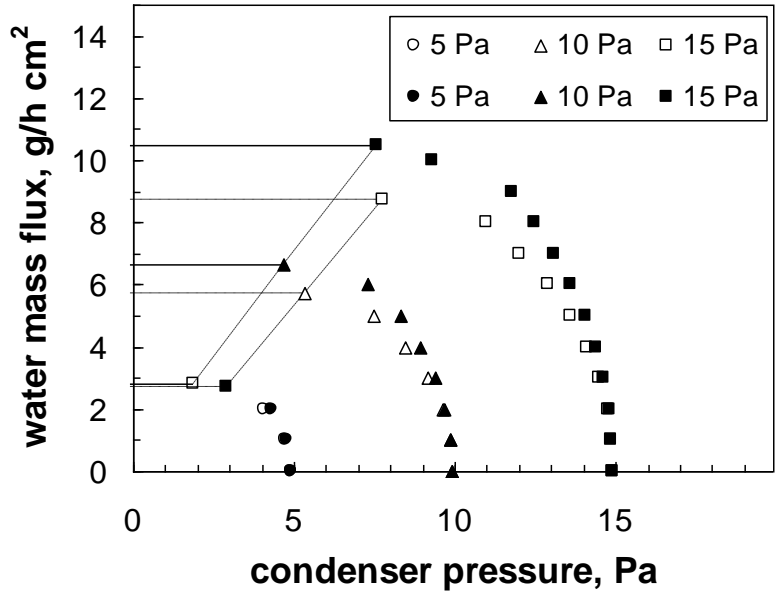
Figure 3. a) Maximum water mass flux in straight ducts of different *L/D* ratio as a function of the chamber pressure. b) Design chart for butterfly valves: mass flux *vs*. outlet pressure, for different inlet pressures. Different disk shapes: open symbols, profiled disk; filled symbols, flat disk. (calculated from DN 700 simulations, with no-slip and adiabatic wall boundary conditions)
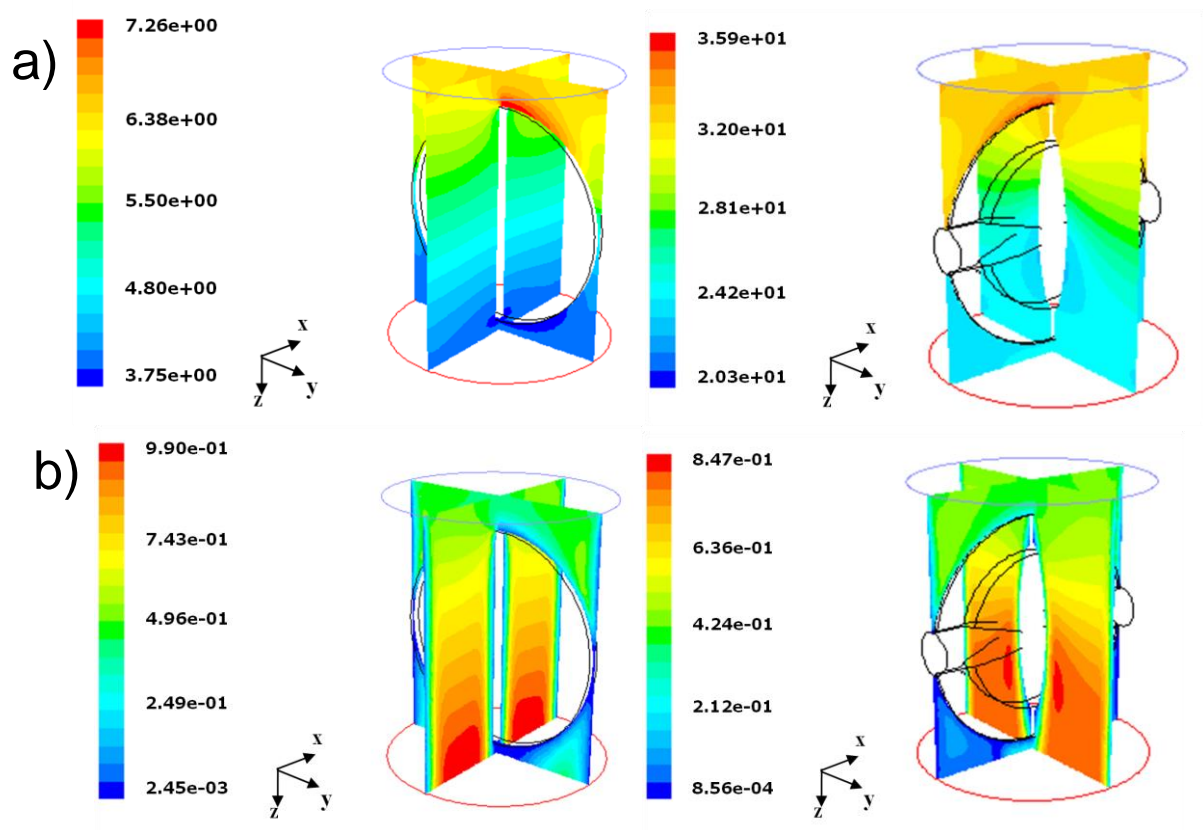
Figure 4. CFD results for the flow trough a butterfly valve with flat disk (left; boundary conditions: no slip and adiabatic wall) and profiled disk (right; boundary conditions: low pressure slip and adiabatic wall). From top to bottom, contours of: a) absolute pressure (Pa); b) Mach number (dimensionless).
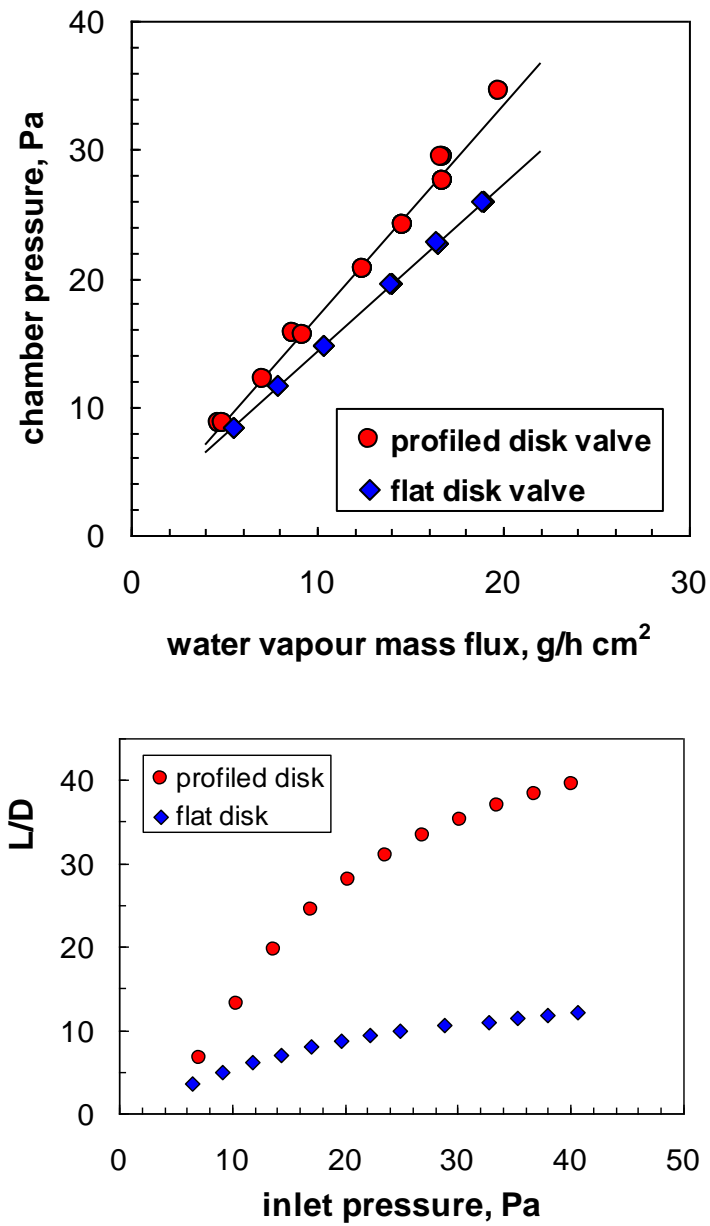
Figure 5. Upper graph: critical water mass flux as a function of the chamber pressure for butterfly valves with different disk profiles (calculated from DN 700 simulations).
Lower graph: equivalent length of the butterfly valves with different disk profile in the choked flow regime, as a function of the inlet (chamber) pressure.
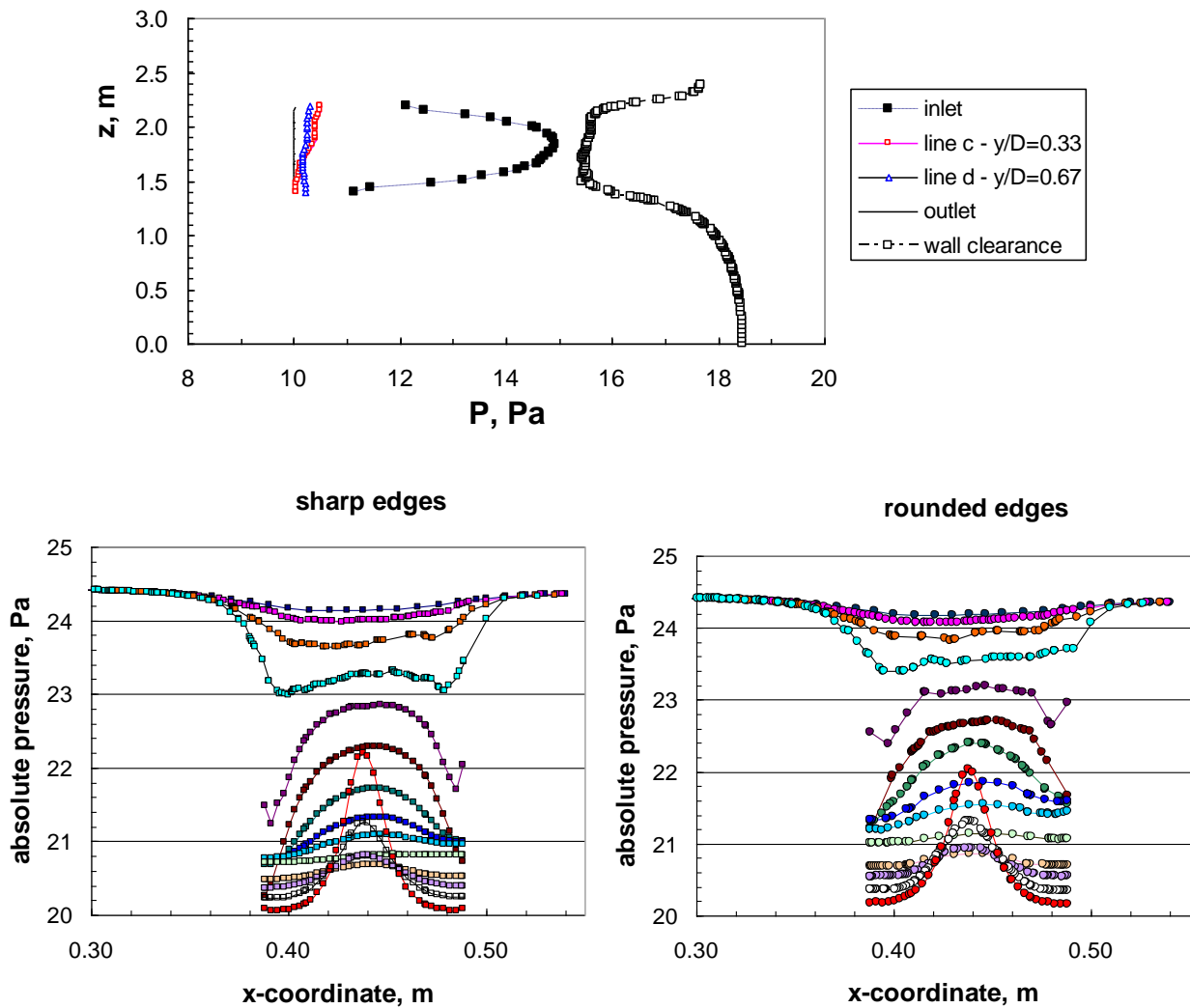
Figure 6. Upper graph: radial profiles of local absolute pressure in the horizontal duct of the large industrial freeze-dryer at different dimensionless distances from the inlet (y/D); the vertical profile in the chamber, in the middle plane of clearance between shelves and wall is also shown. The vapour flow rate corresponds to maximum sublimation rate (1 kg h^{-1} m^{-2}) in the L4 configuration (17 shelves); an outlet pressure of 10 Pa is set. The corresponding radial velocity profiles and the pressure profile along the duct axis are shown in Figure 23 (Barresi and Marchisio, 2018).

Bottom graphs: radial profiles of local absolute pressure in the first part of the duct connecting the chamber of the small pilot scale freeze-dryer (*LyoBeta*^{TM} by Telstar) with the butterfly valve: square symbols, sharp inlet edge (left graph); circle symbols, rounded inlet edge (right graph). The four top lines show the pressure profile on the same plane in the clearance between the bottom shelf and the bottom wall in the chamber. The vapour flow rate corresponds to maximum sublimation rate (1 kg h^{-1} m^{-2}) on the four shelves, with a 5% mass fraction of inert gas. The whole chamber-duct-condenser in modelled; an outlet condenser pressure of 4 Pa is set.
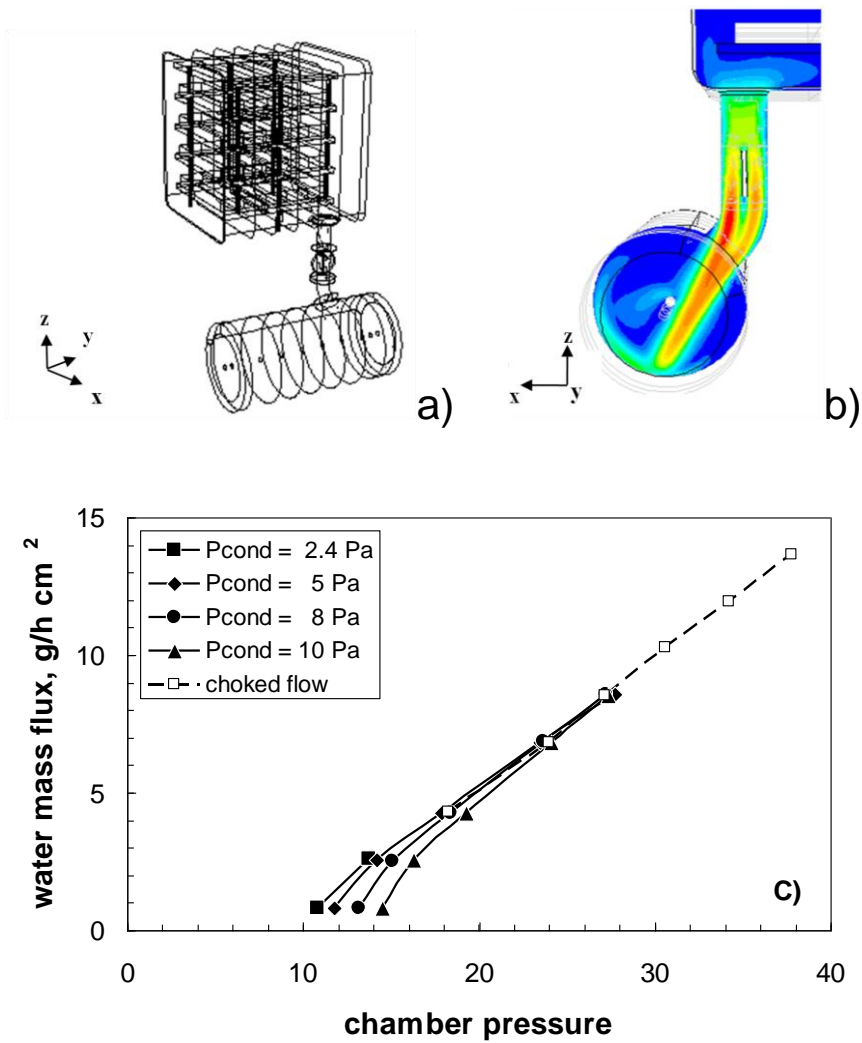
Figure 7. Simulations for the real duct and butterfly geometry in the lab-scale apparatus. a) Geometry of the whole apparatus, including chamber, duct with rounded entrance and condenser. b) Contours of the Mach number on the middle plane passing through the duct, for 1 kg h^{-1} m^{-2} sublimation rate, 5% inert gas fraction and outlet condenser pressure = 4 Pa. For these conditions a maximum value of 0.84 (red zone) is observed for the flow behind the valve restriction. c) Water mass flux as a function of the chamber and condenser pressure, for a flow containing 5% of nitrogen; conditions corresponding to choked flow (open symbols) are also shown.
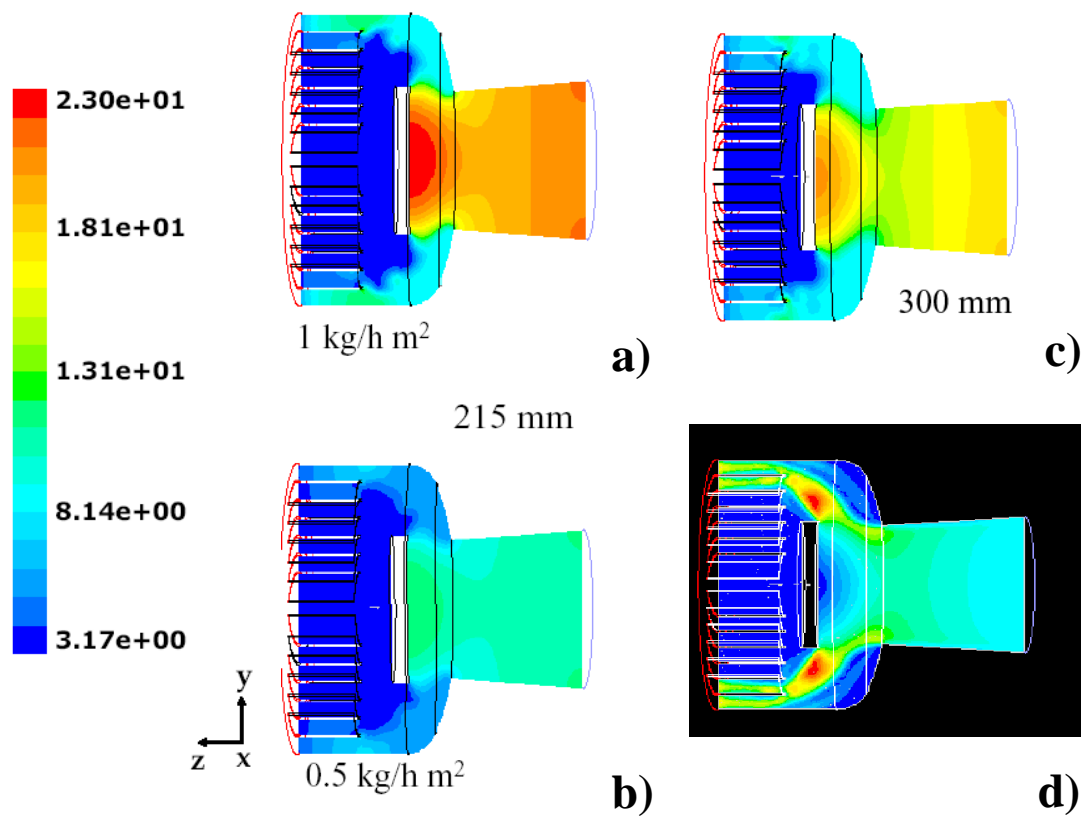
Figure 8. Mushroom valve: absolute pressure in the inlet zone of the condenser on plane $x=0$ for different values of the sublimating rate (17 sublimating shelves) and valve distance: a) l_{valve}=215 mm, sublimating rate = 1 kg h^{-1} m^{-2}; b) l_{valve}=215 mm, sublimating rate = 0.5 kg h^{-1} m^{-2}; l_{valve}=300 mm, sublimating rate = 1 kg h^{-1} m^{-2}. d) Contour plot showing the Mach number distribution (l_{valve} = 300 mm; sublimation rate = 1 kg/h m^2): yellow zones correspond to Mach=1, while in red zones Mach reaches 1.8.
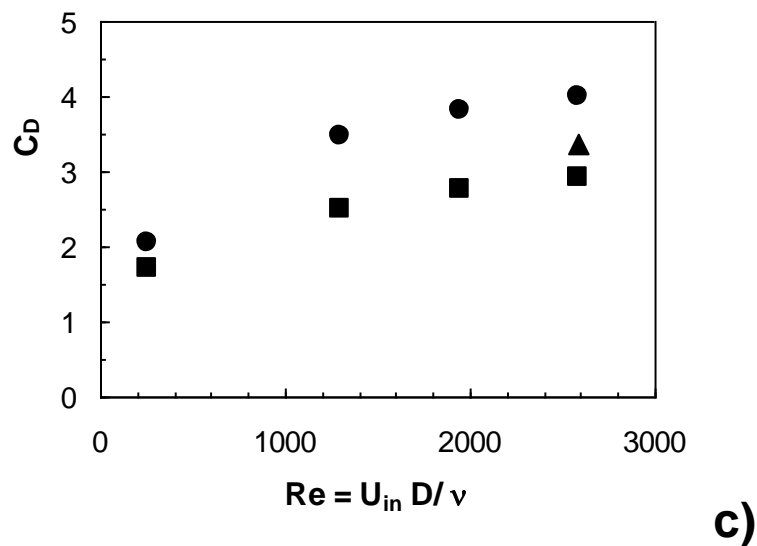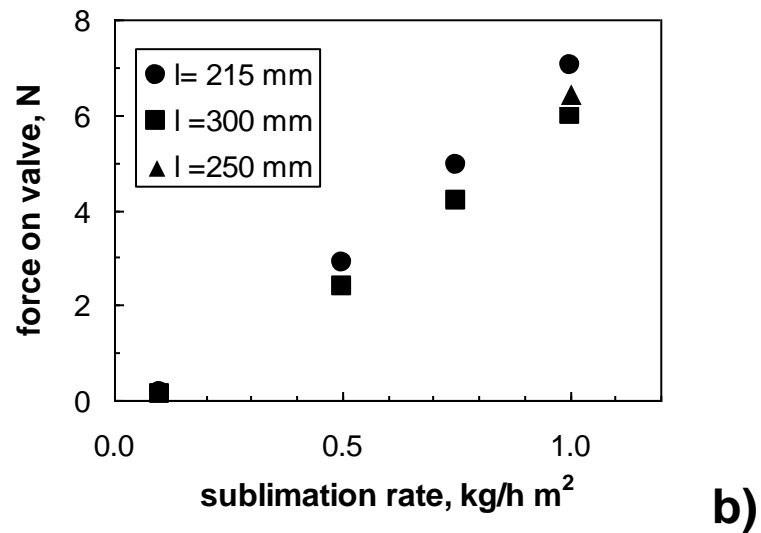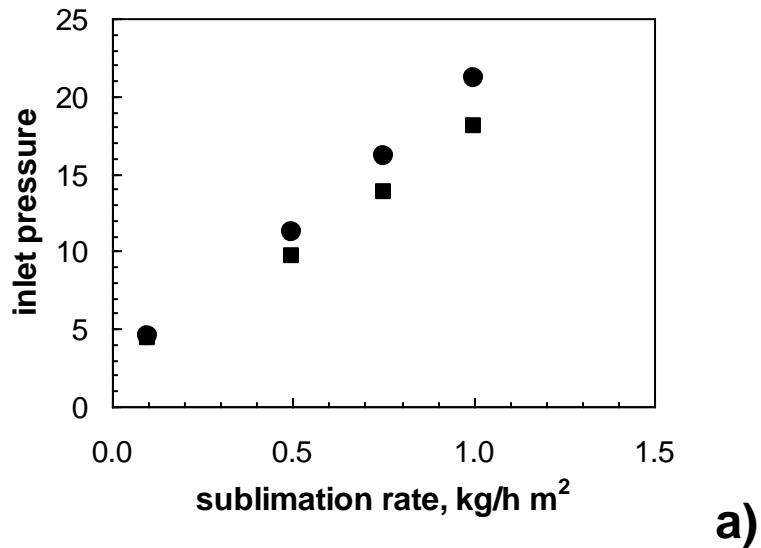
Figure 9. Mushroom valve. a) Required inlet pressure (for a condenser pressure = 4 Pa) as a function of the sublimation rate in the industrial scale freeze-dryer chamber, for different values of the disk valve distance (in mm). b) Force on the valve disk, as a function of the sublimation rate, for different valve disk distances (in mm). c) Drag coefficient *vs*. Reynolds number for the disk of the mushroom valve.